2003 SCEC Progress Report

Fully Three-Dimensional, Multi-Scale Waveform Tomography for the Los Angeles Basin

Principal Investigator:	Li Zhao
Co-Investigators:	Po Chen (USC) Thomas H. Jordan (USC) Kim B. Olsen (UCSB)
Institution:	University of Southern California

Proposal category:	Integration and Theory
Focus group:	Ground Motion

Progress report: Fully three-dimensional, multi-scale waveform tomography for the Los Angeles Basin

Li Zhao, Po Chen, Thomas H. Jordan and Kim B. Olsen

1. Summary of research project

In order to make physics-based strong-motion predictions for earthquake hazard assessments in the Los Angeles area, it is crucial for us to have a good knowledge of the three-dimensional (3-D) regional subsurface structure. We have proposed to carry out a fully 3-D tomography study for the Los Angeles region using the SCSN records from local earthquakes (Fig.1). Our objective is to make quantitative assessments of the current regional models such as the SCEC community velocity model (SCEC CVM 3.0) and then improve the model. We achieve this goal by a) making waveform-based and frequency-dependent measurements of phase and amplitude anomalies such that more information can be extracted from records; b) developing numerical tools for computing the Fréchet kernels of the measurements using fully 3-D reference models without invoking the high-frequency and/or structural averaging approximations that are commonly used in seismic tomography at both global and regional scales; c) using the measurements and the Fréchet kernels to make quantitative assessments of the SCEC reference model; and d) conducting the inversions in a multi-scale fashion, starting from lower frequency and inverting for larger-scale structures, and progress to higher frequencies and smaller-scale structures to ensure the linear dependence of the data on structural perturbations. In this approach, frequency-dependent phase and amplitude anomalies of the first as well as the later arrivals are measured by the same method. The measurements are related to the structural perturbations by accurate and realistic Fréchet kernels. As a result, this approach is particularly suitable for inverting for the shear-speed structure that can only be constrained by later arrivals. This tomography project is a component of a unified approach we are developing to analyze and invert waveform-derived measurements for small-scale regional structure and source processes of small earthquakes. So far we have made significant progress on Items (a)-(c) and we are now ready to conduct a full 3-D tomography study for the region around the L. A. Basin. This report will focus on the aspect of 3-D Fréchet kernels (Item b) with a brief discussion of the measurement process (Item a) and the application of the kernels in the assessment of the SCEC CVM (Item c). Details on Items (a) and (c) can be found in the report by Jordan et al. (2003a).

2. Generalized seismological data functionals (GSDF)

Our unified approach is based on the starting or reference models for the structure and the source and seeks to find out the imperfections of the models by inverting the discrepancy between the model predicted seismic waveforms and the recorded ones. For an earthquake at $\mathbf{r}_S$ and a station at $\mathbf{r}_R$, we can express the model predicted seismic waveform as

$$u_0(\mathbf{r}_R, \omega; \mathbf{r}_S) = \sum_{n=1}^{N} u_0^n(\mathbf{r}_R, \omega; \mathbf{r}_S) = \sum_{n=1}^{N} \exp[i\omega\, t_p^n(\mathbf{r}_R, \omega; \mathbf{r}_S) - \omega\, t_q^n(\mathbf{r}_R, \omega; \mathbf{r}_S)], \quad (1)$$

where the seismogram is regarded as a superposition of a series of constituents such as the waveforms from a series of seismic body waves (e.g. *P* and *S* waves, etc) or a number of surface-

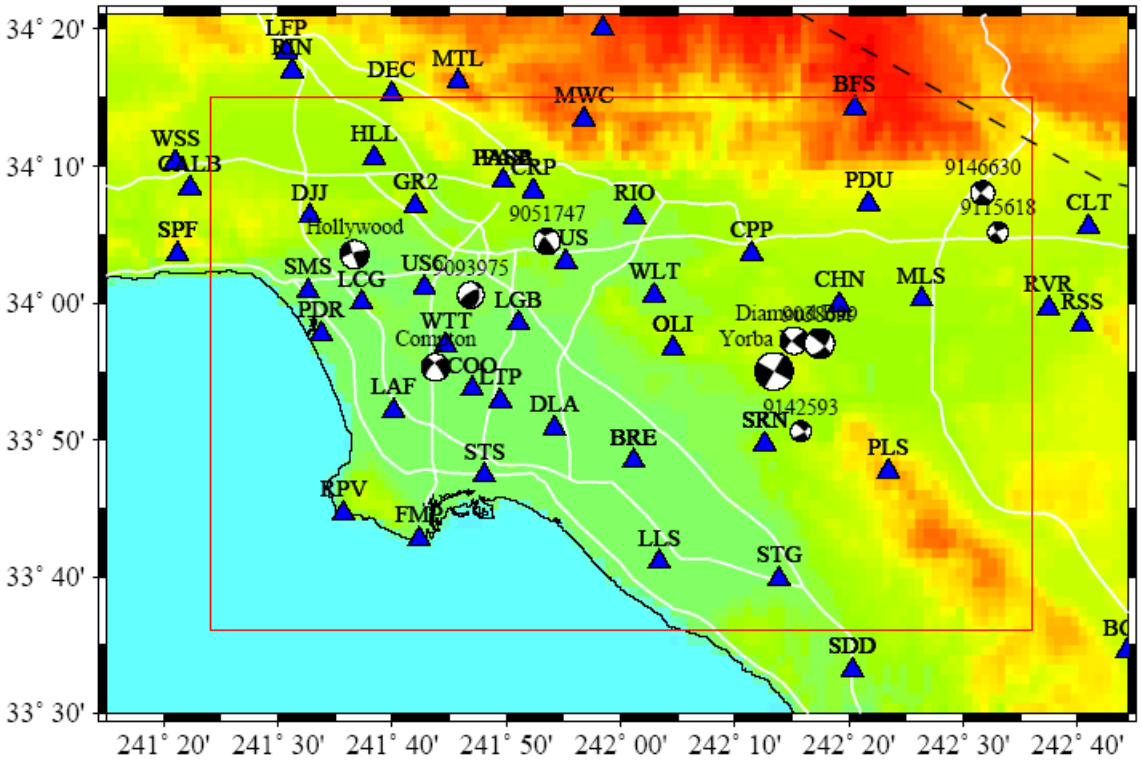

Figure 1. Topography map of the L. A. Basin region. The blue triangles are the locations of SCSN stations. The red rectangle shows the region in which the finite-difference simulations are conducted. Used in the assessment of the 3-D mode SCEC CVM 3.0 are the 34 stations and 10 earthquakes whose locations and focal mechanisms are shown by the beachballs.

wave modes (e.g. fundamental and overtone branches) or arbitrary unnamed signals in the seismogram. The phase and amplitude of each of these constituent waveforms can be described by the two frequency-dependent quantities, $t_p^n(\mathbf{r}_R,\omega;\mathbf{r}_S)$ and $t_q^n(\mathbf{r}_R,\omega;\mathbf{r}_S)$, respectively, both of which have the unit of time. Due to the imperfections of the starting structure and source models, the waveform actually recorded at the station can be written as

$$\begin{aligned} u(\mathbf{r}_R,\omega;\mathbf{r}_S) &= \sum_{n=1}^{N} u_0^n(\mathbf{r}_R,\omega;\mathbf{r}_S)\exp[i\omega\,\delta t_p^n(\mathbf{r}_R,\omega;\mathbf{r}_S) - \omega\,\delta t_q^n(\mathbf{r}_R,\omega;\mathbf{r}_S)] \\ &= \sum_{n=1}^{N} \exp\{i\omega[\,t_p^n(\mathbf{r}_R,\omega;\mathbf{r}_S) + \delta t_p^n(\mathbf{r}_R,\omega;\mathbf{r}_S)] - \omega\,[t_q^n(\mathbf{r}_R,\omega;\mathbf{r}_S) + \delta t_q^n(\mathbf{r}_R,\omega;\mathbf{r}_S)]\}. \end{aligned} \tag{2}$$

where $\delta t_p^n(\mathbf{r}_R,\omega;\mathbf{r}_S)$ and $\delta t_q^n(\mathbf{r}_R,\omega;\mathbf{r}_S)$ are the phase delays and amplitude reductions, respectively, of the constituent waves. They can be linearly related to the source and structural model perturbations and they are defined such that their positive values indicate delays in arrival times and decreases in amplitudes. In practice, it is often impossible to separate in the seismograms the different constituent waves, therefore the individual phase delays and amplitude reductions on the right-hand-side of eq.(2) can not be directly measured. However, as discussed in Jordan et al. (2003a), the method of generalized seismological data functionals (GSDF) first introduced in Gee & Jordan (1992) provides a mechanism for making the Rytov-type frequency-dependent measurements of the discrepancy between the recorded and model-predicted waveforms, i.e. the left-hand-sides of eqs. (1) and (2), and expressing these measurements as

linear combinations of the individual phase delays and amplitude reductions. As a result, the frequency-dependent GSDFs can be used to linearly invert for the source and structural model perturbations. The finite moment tensors are inverted using the partial derivatives of the GSDFs and will be discussed in Jordan et al. (2003b). The tomography is conducted using the structural sensitivity functions or the Fréchet kernels of the GSDFs and will be the focus of this report.

3. Fully 3-D Fréchet kernels

As mentioned before, our data in structural inversion are measured with the GSDF method and are linear combinations of individual phase delays and amplitude reductions $\delta t_p^n(\mathbf{r}_\mathrm{R},\omega;\mathbf{r}_\mathrm{S})$ and $\delta t_q^n(\mathbf{r}_\mathrm{R},\omega;\mathbf{r}_\mathrm{S})$. Thus, the Fréchet kernels for the GSDF data are also linear combinations of the Fréchet kernels for the individual phase delays and amplitude reductions with the same coefficients. The Fréchet kernel for a given phase delay or amplitude reduction is defined as:

$$\delta t_d(\mathbf{r}_\mathrm{R},\omega;\mathbf{r}_\mathrm{S}) = \int_\oplus K_d^m(\mathbf{r}_\mathrm{Q};\mathbf{r}_\mathrm{R},\omega;\mathbf{r}_\mathrm{S})\delta m(\mathbf{r}_\mathrm{Q})\, d^3\mathbf{r}_\mathrm{Q}, \tag{3}$$

where d indicates the type of the data and m represents any model parameter (such as P-wave speed α) with perturbation δm. The integral is over the entire volume of interest. The 3-D function $K_d^m(\mathbf{r}_\mathrm{Q})$ is the so-called Fréchet kernel which represents the sensitivity of the seismic datum d to the local perturbation in model parameter m.

In the integral relation in eq.(3), there are three spatial functions involved in the integrand, including the Fréchet kernel $K_d^m(\mathbf{r}_\mathrm{Q})$, the model perturbation δm, and the reference model m_0 in which the kernels are computed. The computations involved in eq.(3) are very intensive when the kernels and the model perturbation vary in three dimensions and can become prohibitively heavy when the reference model is also 3-D since the kernels can only be obtained purely numerically. As a result, all current seismic tomography studies are not fully 3-D in the sense that the reference mode is always 1-D and the Fréchet kernels are also approximated by 1-D or 2-D functions. Further approximations are often adopted so that the kernels are computed by simple methods such as the geometrical ray theory. In all cases, the simplifications amount to a structural averaging assumption that requires the wavelength of the seismic waves used to be much shorter than the typical length scale of the structural heterogeneities. As the scale of the inhomogeneity approaches the wavelength of the studied seismic waves, the averaging approximations are no longer valid and the Fréchet kernels are intrinsically 3-D and they must be calculated using accurate wave-propagation methods. In our 3-D tomography study for the L. A. Basin where we hope to achieve a resolution of a few kilometers, it is important to use 3-D Fréchet kernels obtained by accurate numerical algorithms without structural averaging approximations. We use the staggered-grid finite-difference method (Olsen 1994). Therefore, our tomography approach uses a 3-D reference model and 3-D Fréchet kernels to invert for 3-D model perturbations. We call this approach the fully 3-D approach.

For an arrival limited in a time window $[t_1,t_2]$, the phase delay and amplitude reduction measured around frequency ω_j can be expressed as (Zhao & Jordan 1998; Dahlen et al. 2000):

$$\delta t_p(\omega_j) = -\frac{\int_{t_1}^{t_2} \dot{u}_0(t)\delta u(t)dt}{\int_{t_1}^{t_2} |\dot{u}_0(t)|^2\, dt}, \quad \delta t_q(\omega_j) = -\frac{1}{\omega_j}\frac{\int_{t_1}^{t_2} u_0(t)\delta u(t)dt}{\int_{t_1}^{t_2} |u_0(t)|^2\, dt}, \tag{4}$$

where a dot represents the time derivative, and the displacement perturbation $\delta u(t)$ can be written as an integral over the volume of the earth model under study:

$$\delta\mathbf{u}(\mathbf{r}_\mathrm{R},t;\mathbf{r}_\mathrm{S}) = -\int_\oplus\int_{-\infty}^{\infty}\mathbf{G}(\mathbf{r}_\mathrm{R},\tau;\mathbf{r})\cdot\left\{\delta\rho(\mathbf{r})\frac{\partial^2}{\partial\tau^2}\mathbf{I}-\nabla\cdot[\delta\mathbf{C}(\mathbf{r})\cdot\nabla]\right\}\cdot\mathbf{u}(\mathbf{r},t-\tau;\mathbf{r}_\mathrm{S})d\tau\,d^3\mathbf{r}, \qquad (5)$$

where $\delta\rho$ and $\delta\mathbf{C}$ are the perturbations in density and the second-order elastic tensor, respectively. $\mathbf{G}(\mathbf{r}_\mathrm{R},\tau;\mathbf{r})$ is the Green's tensor from $\mathbf{r}$ to receiver $\mathbf{r}_\mathrm{R}$ in the reference model, $\mathbf{u}(\mathbf{r},t-\tau;\mathbf{r}_\mathrm{S})$ is the displacement from earthquake source at $\mathbf{r}_\mathrm{S}$ to $\mathbf{r}$ in the perturbed model, and $\mathbf{I}$ is the second-order identity tensor. An integration by parts in eq.(5) will eliminate the terms with spatial gradients of the model perturbations. From eqs.(3), (4) and (5), we can derive the expressions for the Fréchet kernels of the individual phase delays and amplitude reductions for P and S wave speeds:

$$K_p^\alpha(\mathbf{r}) = -\frac{2}{P}\int_{t_1}^{t_2}\rho_0\alpha_0\dot{u}_0(\mathbf{r}_\mathrm{R},t;\mathbf{r}_\mathrm{S})\int_{-\infty}^{\infty}\hat{\mathbf{e}}_l\cdot[(\nabla\cdot\mathbf{G}^\mathrm{T})(\nabla\cdot\mathbf{u}_0)]\,d\tau\,dt, \qquad (6)$$

$$K_q^\alpha(\mathbf{r}) = -\frac{2}{Q}\int_{t_1}^{t_2}\rho_0\alpha_0 u_0(\mathbf{r}_\mathrm{R},t;\mathbf{r}_\mathrm{S})\int_{-\infty}^{\infty}\hat{\mathbf{e}}_l\cdot[(\nabla\cdot\mathbf{G}^\mathrm{T})(\nabla\cdot\mathbf{u}_0)]\,d\tau\,dt, \qquad (7)$$

$$K_p^\beta(\mathbf{r}) = \frac{2}{P}\int_{t_1}^{t_2}\rho_0\beta_0\dot{u}_0(\mathbf{r}_\mathrm{R},t;\mathbf{r}_\mathrm{S})\int_{-\infty}^{\infty}\hat{\mathbf{e}}_l\cdot\{(\nabla\mathbf{G})^{213}:[(\nabla\mathbf{u}_0)+(\nabla\mathbf{u}_0)^\mathrm{T}]-2(\nabla\cdot\mathbf{G}^\mathrm{T})(\nabla\cdot\mathbf{u}_0)\}\,d\tau\,dt, \qquad (8)$$

$$K_q^\beta(\mathbf{r}) = \frac{2}{Q}\int_{t_1}^{t_2}\rho_0\beta_0 u_0(\mathbf{r}_\mathrm{R},t;\mathbf{r}_\mathrm{S})\int_{-\infty}^{\infty}\hat{\mathbf{e}}_l\cdot\{(\nabla\mathbf{G})^{213}:[(\nabla\mathbf{u}_0)+(\nabla\mathbf{u}_0)^\mathrm{T}]-2(\nabla\cdot\mathbf{G}^\mathrm{T})(\nabla\cdot\mathbf{u}_0)\}\,d\tau\,dt, \qquad (9)$$

where $\hat{\mathbf{e}}_l$ is the unit vector in the direction of the $u_0(t)$ polarization. The superscript T represents the transpose of a second-order tensor. The symbol $(\cdot)^{213}$ represents the transposing of the first and the second indices of a third-order tensor. The normalization factors are

$$P = \int_{t_1}^{t_2}|\dot{u}_0(t)|^2\,dt, \text{ and } Q = \omega_j\int_{t_1}^{t_2}|u_0(t)|^2\,dt. \qquad (10)$$

Note that in these expressions, $\mathbf{G}(\mathbf{r}_\mathrm{R},t;\mathbf{r})$ is the Green's tensor from $\mathbf{r}$ to $\mathbf{r}_\mathrm{R}$ and $\mathbf{u}_0(\mathbf{r},t;\mathbf{r}_\mathrm{S})$ is the displacement from $\mathbf{r}_\mathrm{S}$ to $\mathbf{r}$. Both are evaluated in the reference model.

4. Implementation of the algorithm

In last year's report, we presented preliminary numerical results for the Fréchet kernels of the phase delays from the implementation of eqs.(6) and (8). A fourth-order staggered-grid finite-difference method (Olsen 1994) and the SCEC CVM 3.0 (Magistrale et al. 2003) were used to compute the wavefields. The code was adapted so that the Green's functions, the responses to single point force instead of double-couple sources, can be calculated. Since each finite-difference modeling provides the three-component velocity responses at all the grid points from one specific source, the wavefield $\mathbf{u}_0(\mathbf{r},t;\mathbf{r}_\mathrm{S})$ in eqs.(6) and (8) can be obtained by a single finite-difference simulation. However, the Green's tensor $\mathbf{G}(\mathbf{r}_\mathrm{R},t;\mathbf{r})$ represents the wavefield at the receiver from sources at all the grid points and requires the same number of finite-difference simulations as the number of grid points, which is an impossible task in practice. Fortunately, the reciprocity principle states that $\mathbf{G}(\mathbf{r}_\mathrm{R},t;\mathbf{r}) = \mathbf{G}^\mathrm{T}(\mathbf{r},t;\mathbf{r}_\mathrm{R})$, which allows us to obtain the Green's

tensor from only three finite-difference simulations with three single point forces in orthogonal directions at the receiver location. Therefore, for each chosen $\hat{\mathbf{e}}_i$, i.e. for each component of the seismogram, only four finite-difference simulations are required to obtain all the Fréchet kernels. The time-domain velocity responses obtained from the finite-difference modeling are then transformed into the frequency domain where the displacement versions of the wavefields are obtained, and the gradients of $\mathbf{G}$ and $\mathbf{u}_0$ are calculated by numerical differentiation. Finally, the right-hand-sides of eqs.(6) and (8) are evaluated to obtain the Fréchet kernels of the phase delays for *P* and *S* wave speeds.

We have now completed the implementation and refinement of the algorithm for computing the Fréchet kernels of the phase delays as well as the amplitude reductions in eqs.(6)-(9). The program has also been explicitly parallelized with OpenMP to run on SMP systems. Using eight processors, on a 250x150x100 spatial grid, it takes about 3 hrs to compute the Fréchet kernels of all the frequency-dependent phase and amplitude measurements that can be obtained on the three components of the seismic record at a station from an earthquake, i.e., up to a total of ~100 kernels when the measurements are taken at five frequencies for *P*, *S* and surface waves on each component. Here we present numerical examples of delay time and amplitude reduction kernels for the Yorba Linda earthquake. Fig.2 shows the basin depth and locations of the epicenter and stations WLT, DLA and LAF. Fréchet kernels at the WLT and LAF are shown in Figs.3 and 4.

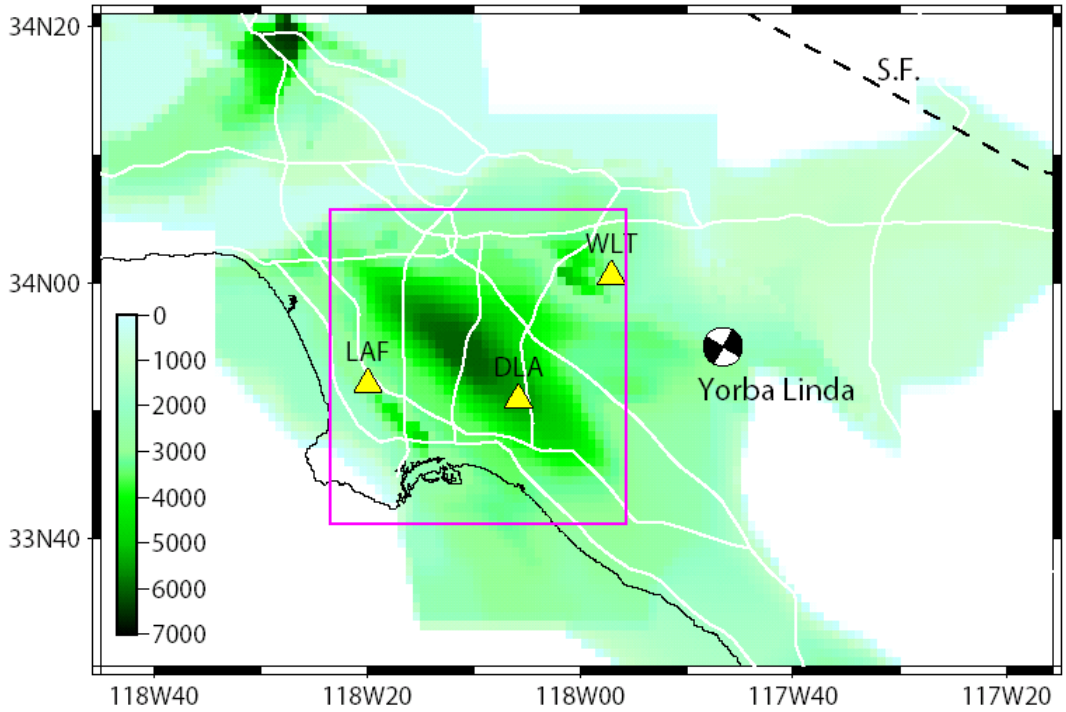

Figure 2. Regional basin depth map (color scale in meters). The location and focal mechanism of the Sept. 3, 2002, Yorba Linda earthquake are shown by the beachball. The yellow triangles show the locations of three SCSN stations. Fréchet kernels at stations WLT and LAF are shown in Figs.3-5.

5. Assessment of SCEC CVM 3.0 using finite-difference synthetics and Fréchet kernels

In addition to developing the algorithm for computing the 3-D Fréchet kernels, we also conducted extensive finite-difference simulations using the 3-D basin model SCEC CVM 3.0.

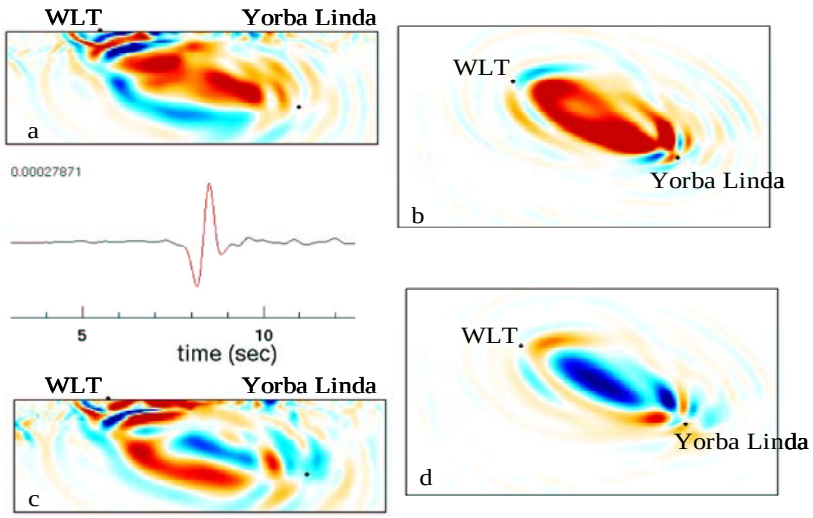

Figure 3. W-E component synthetics seismogram from Yorba Linda to WLT and the kernels for the *S* wave. (a) Travel-time kernel for β in source-station vertical plane. Warm and cool colors indicate advance and delay, respectively, for a velocity increase. (b) The same travel-time kernel in the horizontal plane at a depth of 6 km. (c,d) Amplitude kernel for β in source-station vertical plane and the horizontal plane at a depth of 6 km. Warm and cool colors indicate amplitude increase and reduction, respectively, for a velocity increase.

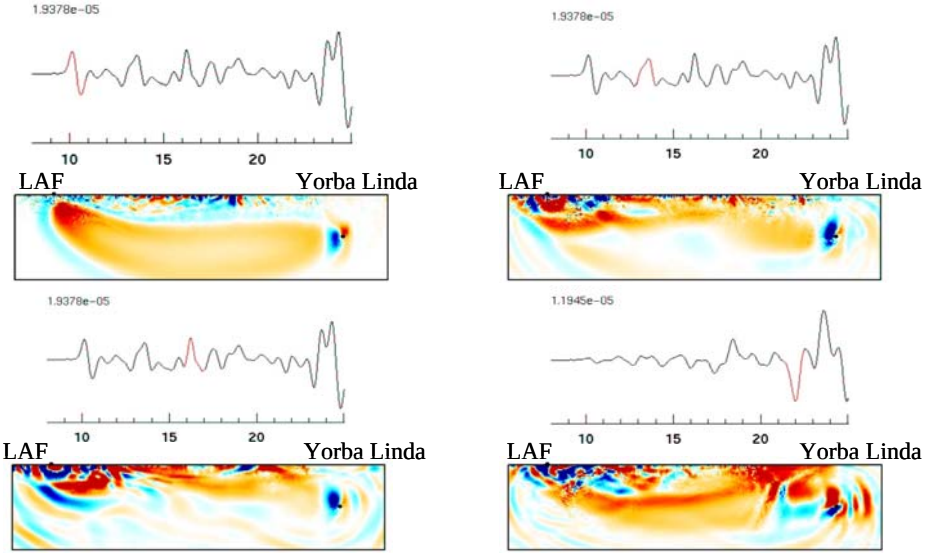

Figure 4. Synthetics seismogram from Yorba Linda to LAF and the travel-time kernels in source-station vertical plane. (Upper left) Kernel for α for the *P* wave. (Upper right) Kernel for α for the arrival around 13 sec. (Bottom left) Kernel for α for the arrival around 16 sec. (Bottom right) Kernel for β for the *S* wave.

We measured the phase delays and amplitude reductions between the synthetics with recorded seismograms and made quantitative assessment of the SCEC velocity model. The region of our FD simulations is shown in Fig.1. Using nearly 400 waveforms at 34 stations and 10 earthquakes we obtained ~4000 GSDF data. Examples of the synthetics and recorded waveform comparisons, quantitative measurements and their statistics can be found in Jordan et al. (2003a).

An important conclusion in the assessment of SCEC CVM 3.0 is that the velocity in this 3-D model is much too slow inside the L. A. Basin. Although this conclusion has been reached from the statistical analysis of the ~4000 GSDF measurements, the 3-D Fréchet kernel for a particular data can often provide important intuition as to where in the model the contribution may come

from. This is demonstrated by the striking example for the phase-delay kernel between the Yorba Linda earthquake and station DLA shown in Fig.5. The waveform comparison and GSDF measurements show that at station DLA the *P* wave predicted by SCEC CVM 3.0 arrives later than that in the record, indicating that the structure around the entire *P* wave path from Yorba Linda to DLA is on average too slow. The kernel for the *P*-wave phase delay shows an extremely enhanced sensitivity in the L. A. Basin near DLA, which strongly suggests that this slow velocity occurs most likely in the Basin. This example demonstrates that the 3-D Fréchet kernel can be a very powerful tool in seismic data interpretation and improving the spatial resolution in tomography inversions.

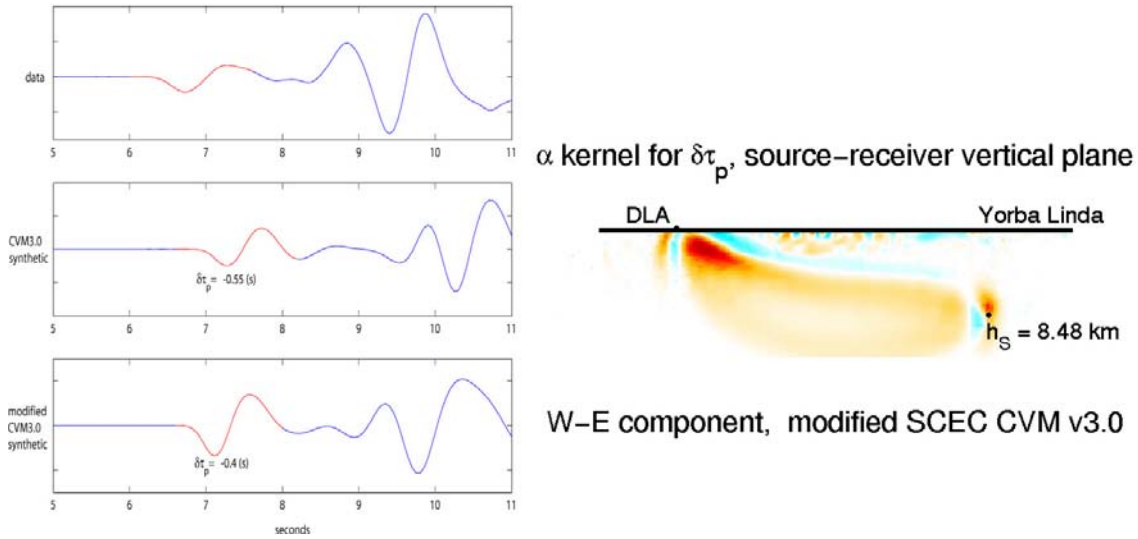

Figure 5. (Left) W-E component record at stations DLA (top) and finite-difference synthetics in two modified versions of SCEC CVM3.0 with minimum shear-wave speed of 1250 m/s (middle) and 2500 m/s (bottom). (Right) Phase-delay Fréchet kernel for α shows that the contribution to phase-delay anomaly comes mostly from the basin near the station (see Fig.2 for the basin location). The travel time anomaly of about -0.55 s suggests that SCEC CVM3.0 is too slow in the basin.

6. Four-dimensional (4-D) visualization of Fréchet kernels

In the past year, we also worked closely with the SCEC ITR project in using the graphics softwares developed by Marcus Thiebaux of the Information Sciences Institute to visualize the large 4-D datasets generated by the Fréchet kernels. Fig.6 is an example in which the 4-D visualization helps us to achieve a clear view of the complex sensitivity distribution of a seismic arrival generated by the 3-D structure. The ability to calculate and visualize the Fréchet kernels in 4-D represents the most exciting advancement in our understanding of the seismic wave propagation and interaction in realistic 3-D heterogeneous structures and will be extremely useful to our research in the future. See http://epicenter.usc.edu/cmeportal/viz.html for details.

Figure 6. (Next page) Vertical component record from Yorba Linda to station DLA and the finite-difference synthetic for SCEC CVM 3.0. Also shown are f-k synthetics in two 1-D models. SCEC 1D is a 1-D path average model between Yorba Linda and DLA, and SoCal is the 1-D model of Dreger and Helmberger (1993). Phase X can be seen clearly in the record and the 3-D synthetic but not in the 1-D synthetics, indicating that its energy comes from scattering by 3-D heterogeneity. In the 10 snapshot taken from an animation of the Fréchet kernel for the X phase, it can be seen that this phase is likely the result of a *P*-to-Rayleigh wave scattering near the surface.

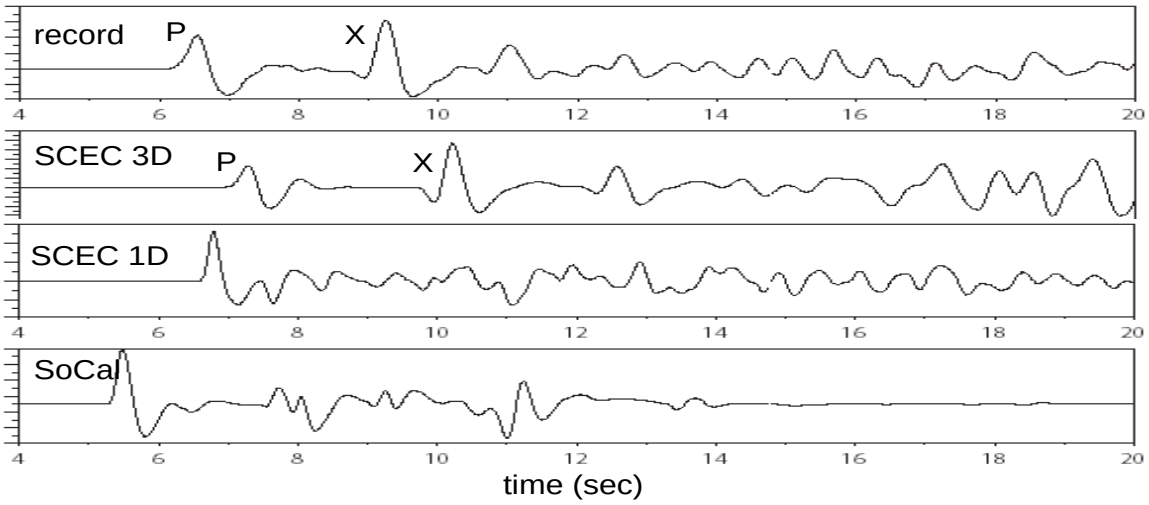
record
P
X
SCEC 3D
P
X
SCEC 1D
SoCal
4
6
8
10
12
14
16
18
20
time (sec)

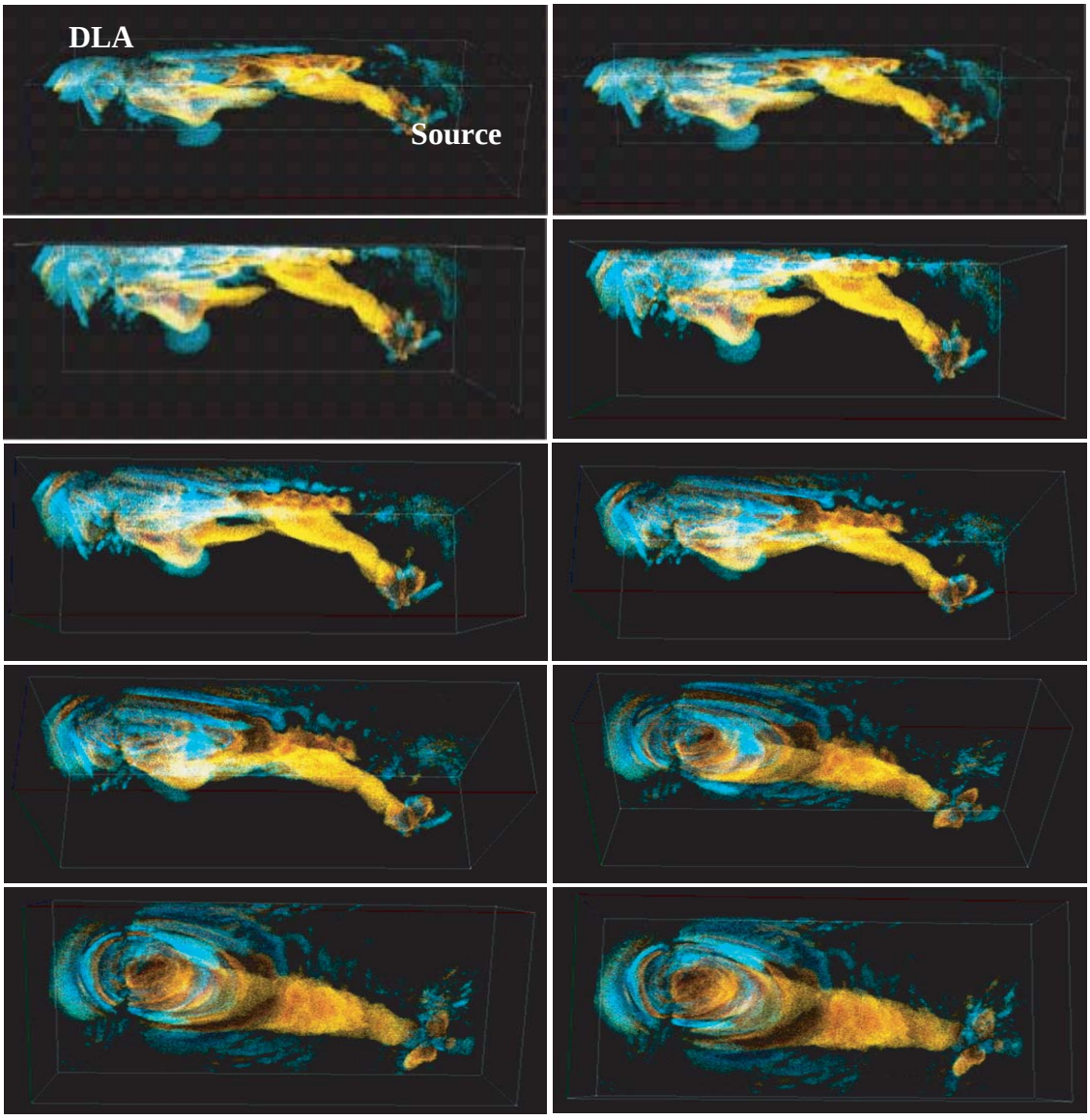
DLA
Source